Long-range atomic ordering and variable interlayer interactions in two overlapping graphene lattices with stacking misorientations

Taisuke Ohta,[1,*] Thomas E. Beechem,[1] Jeremy T. Robinson,[2] and G. L. Kellogg[1]
[1]*Sandia National Laboratories, Albuquerque, New Mexico 87185, USA*
[2]*Naval Research Laboratory, Washington, DC 20375, USA*
(Received 1 December 2011; published 16 February 2012)

The low-energy electronic dispersion of graphene is extremely sensitive to the nearest layer interaction and thus the stacking sequence. Here, we report a method to examine the effect of stacking misorientation in bilayer graphene by transferring chemical vapor deposited (CVD) graphene onto monolithic graphene epitaxially grown on silicon carbide (SiC) (0001). The resulting hybrid bilayer graphene displays long-range Moiré diffraction patterns having various misorientations even as it exhibits electron reflectivity spectra nearly identical to epitaxial bilayer graphene grown directly on SiC. These varying twist angles affect the 2D (G')-band shape of the Raman spectrum, indicating regions of both a monolayer-like single π state and Bernal-like split π states brought about by the differing interlayer interactions. This hybrid bilayer graphene fabricated via a transfer process therefore offers a way to systematically study the electronic properties of bilayer graphene films as a function of stacking misorientation angle.

DOI: 10.1103/PhysRevB.85.075415 PACS number(s): 61.48.Gh, 61.05.jh, 63.22.Rc

I. INTRODUCTION

Graphene's unique electronic band structure is the genesis for its widespread promise in applications ranging from RF-electronics[1] and photodetectors[2,3] to DNA transcription.[4] The band structure of graphene is not invariant but is instead dependent on the number of layers and the relative arrangement of these layers, i.e., their stacking sequence. Monolayer graphene, for example, is dominated by massless charge carriers arising from the linear dispersion of a single Dirac cone. In contrast, bilayer graphene, when stacked in a Bernal arrangement (e.g., AB stacking as in a graphite crystal), is marked by massive charge carriers described by a quadratic dispersion.[5] Between these extremes, a composite response evolves in so-called "twisted" graphene, in which the stacked layers have a relative in-plane angular misorientation.[6,7] In these twisted films, the angle of rotation determines the characteristics of the band structure, thereby providing an additional "knob" that allows for further engineering of graphene's band structure.

From a theoretical perspective, twisted bilayer graphene (TBG) has been examined extensively using both continuum[6–9] and *ab-initio*[10–14] approaches. These studies have shown that the individual monolayers become significantly decoupled by the rotational faults. This significant, but not necessarily complete, decoupling leads to an electronic dispersion that is monolayer-like in its linearity around the charge-neutrality point (or Dirac point). For rotational angles away from either 0 or 60°, this linearity results in a Fermi velocity nearly equivalent to that of monolayer graphene. From this perspective, twisted graphene should act effectively like a single monolayer.[13] Recent work, however, has shown a more complex response, in which the Fermi velocity is reduced to zero at certain "magic angles" away from either 0 or 60°.[9] This implies that near the Dirac point, the linearity characteristic of monolayer graphene is completely removed.[6] As such, the dispersion is instead more like that of either Bernal or AA stacked graphene, albeit with greatly reduced energy separation between the states. TBG will not, therefore, necessarily respond in a manner analogous to monolayer graphene. Rather, the rotational faults provide a degree of freedom that alters the band structure in a way that is yet to be fully understood.[15,16]

Rotationally faulted structures occur naturally in graphite crystals and during the epitaxial growth of graphene on the C-face (000$\bar{1}$) of SiC.[10,17,18] TBG has also been realized by folding exfoliated graphene atop itself.[19,20] In the case of graphene on SiC (000$\bar{1}$), the angle of rotation between the layers varies with the growth and at present does not provide a means to control the relative misorientation. Folding approaches, meanwhile, provide only one small twisted region with a single misorientation angle. There is, therefore, no adequate form of graphene that lends itself to a systematic study linking physical properties (i.e., electronic dispersion) to specific twist angles.

In response, we fabricated TBG by transferring a monolayer of graphene synthesized by chemical vapor deposition (CVD) onto a monolayer of epitaxially grown graphene on SiC (0001). Due to the polycrystalline nature of CVD graphene, the resulting hybrid bilayer film has several regions with different stacking misorientations, thus allowing for a direct examination into the way in which the twist angle alters the material's properties. Specifically, by utilizing low-energy electron microscopy (LEEM), low-energy electron diffraction (LEED), and Raman spectroscopy, the hybrid twisted bilayers are shown to: (1) intimately adhere to each other, (2) preserve the long-range atomic ordering exhibited in the Moiré structure unique to each twist angle, and (3) induce changes in a Raman scattering process as a result of the electronic coupling between layers. These results establish that a transfer-based approach provides a useful test bed to study the effect of rotational faults, and it also demonstrates promise in realizing graphene multilayers retaining graphene's unique two-dimensional transport characteristics.

II. EXPERIMENT

Hybrid bilayer graphene films were made by transferring a monolayer of graphene formed on copper foil via a CVD

process to the surface of a monolayer of epitaxial graphene grown on a silicon carbide (SiC) (0001) substrate. Epitaxial graphene films grown on SiC(0001) retain their epitaxial relation to the substrate, and therefore they have a unique crystallographic orientation. Graphene derived from a CVD process, in contrast, exhibits micron-scale domains having different orientations relative to the copper surface. Thus, it is expected that by placing the CVD graphene atop the epitaxial graphene, a hybrid bilayer will have regions of varying stacking misorientation. Two varieties of epitaxial graphene on SiC are used for this work: (1) epitaxial graphene retaining an underlying interface carbon (C-) layer (or "buffer" layer) characterized by its $6\sqrt{3} \times 6\sqrt{3}$ cos 30° LEED pattern,[21,22] and (2) quasi–free-standing graphene monolayers made via hydrogen intercalation.[23] Substrate-related LEED spots are absent for the quasi–free-standing films due to the reduced interaction between the graphene and the underlying SiC,[23] making them suitable to study the diffraction patterns of the hybrid films examined here. Synthesis of the epitaxial graphene is described in detail within Refs. 24 and 25.

The monolayer of graphene placed atop these epitaxial layers is grown on a copper foil based on a reported CVD process.[26] Transfer of the CVD graphene film was conducted following typically reported approaches[26] in which a layer of polymethyl methacrylate (PMMA) stabilizes the graphene film as the Cu foil is etched. After transferring the PMMA/graphene film onto the hydrophobic graphene-SiC substrate, the sample is spun at 2000 rpm to remove excess water, heated to 150 °C for 10 minutes, and then soaked in acetone to remove PMMA. We find the spinning step improves film adhesion, especially on hydrophobic surfaces. TBG films are further cleaned by either annealing in ultrahigh vacuum at ∼400 °C for ∼14 hours or in hydrogen (45%)-argon mixture at ∼180 °C for 2 hours. Both cleaning processes yield clean surfaces characterized by sharp LEED patterns with no noticeable difference between the two. Hereafter, the resulting types of bilayer films are referred to as hybrid bilayers on C-layer-terminated SiC (i.e., with buffer layer) and on H-terminated SiC (i.e., without buffer layer), respectively. The graphene grown on SiC is termed as the underlayer, and the transferred CVD graphene is termed as the overlayer.

III. RESULTS

Figure 1(a) shows a LEEM image of a hybrid bilayer film on C-layer-terminated SiC.[27] The dark lines that cross the image at approximately 45° are step bunches, varying from 2 to 20 nm in height, that arise as part of the epitaxial growth process. The image closely resembles previously obtained LEEM images of epitaxially grown monolayer graphene on C-layer-terminated SiC[21] and, along with AFM images (not shown), indicates that the transfer process produces relatively flat surfaces free from significant contamination. The number of graphene layers at any location is deduced from the electron energy dependence of the reflected electron intensity (LEEM-IV spectra). Specifically, the shape of LEEM-IV spectrum in the energy range just above the vacuum cutoff (E_{vac}) is directly correlated with the number of graphene layers. Representative spectra from the C-layer- and H-terminated substrates are shown in Fig. 1(b). The top plot compares the IV spectrum

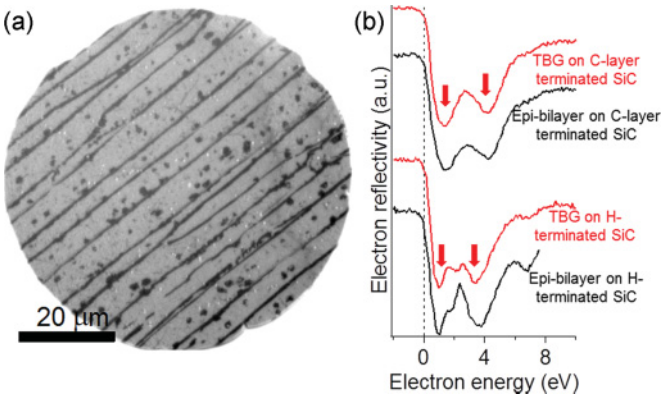

FIG. 1. (Color online) (a) LEEM image of hybrid bilayer graphene films on C-layer-terminated SiC imaged at the electron energy of E_{vac} +3.1 eV. (b) LEEM-IV spectra of hybrid bilayer and epitaxial bilayer graphene on C-layer-terminated and H-terminated SiC. The red arrows highlight the two dips characteristic of bilayer graphene.

from the bright regions of the LEEM image (nominally flat terraces) with that from a previously grown epitaxial bilayer. The two dips, indicated by the two red arrows, are a signature of bilayer graphene films on C-layer-terminated SiC(0001).[28,29] A similar comparison for transferred versus epitaxial bilayer graphene on H-terminated surfaces is shown in the lower trace. For both systems, there is a close match between the spectra, thus providing clear evidence that the transfer process is successful in producing bilayer graphene. Moreover, because the dips in LEEM-IV spectra are due to the quantization of bulk graphite states by the finite film thickness, these results suggest that the interlayer interaction in the hybrid bilayer films is very similar to that of epitaxial bilayer graphene. Thus, intimate binding is established between the graphene overlayer and epitaxial underlayer.

In addition to the step bunches and bright regions (bilayer graphene) in Fig. 1, small dark patches appear every 5–10 μm. LEEM-IV spectra from these regions have the signature of trilayer graphene. These trilayer patches occur where the transferred sheet lies on top of preexisting epitaxial bilayer regions. We have also occasionally observed breaks (or gaps) in the overlayers (not shown in Fig. 1), which are identified as bare epitaxial graphene in LEEM-IV spectra. Additionally, folds in the overlayer were also observed irregularly. The trilayer graphene, breaks, and folds are also seen in the accompanying Raman analysis discussed later in this study.

Ideally, multiple domains with different orientations would be observed so that changes in the electronic structure could be probed as a function of twist angle. Neither LEEM images nor LEEM-IV spectra, however, provide information on the rotational orientation of the transferred film with respect to the epitaxial graphene layer. To then show that we indeed have twisted bilayer domains with varying twist angles, area-selective LEED patterns were obtained from the same surfaces examined using LEEM. Figure 2 shows examples of the resulting LEED patterns from hybrid bilayer films on both C-layer-terminated and H-terminated SiC. The LEED patterns were captured while the sample was moved by ∼500 μm beneath the electron beam. Importantly, as the

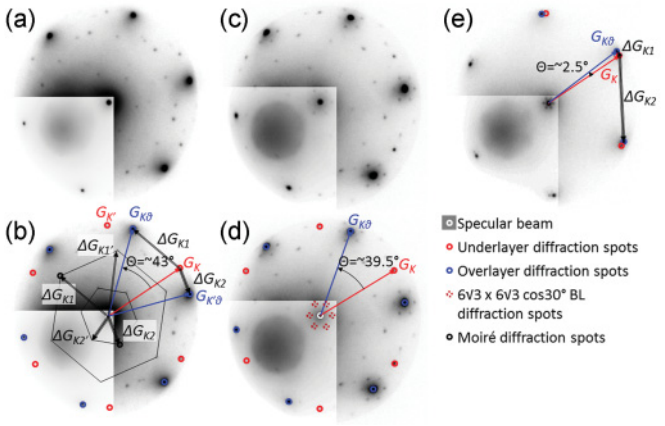

FIG. 2. (Color online) LEED patterns of hybrid bilayer exhibiting the signature of TBG. The image contrast of the lower-left quadrant in each panel is reduced to show the overall symmetry of the patterns. All LEED patterns were acquired from a 5 μm diameter area using an imaging aperture. (a) and (b) LEED patterns of TBG on H-terminated SiC with twist angle of ~43°, measured at an electron energy of E_{vac} +42 eV. (c) and (d) LEED patterns of TBG on C-layer-terminated SiC with twist angle of ~39.5°, measured at the electron energy of E_{vac} +47 eV. (e) LEED pattern of TBG on H-terminated SiC with twist angle of ~2.5°, measured at the electron energy of E_{vac} +42 eV. (b), (d), and (e) illustrate the spot locations (circles), the twist angle, the reciprocal lattice vectors (red and blue arrows), and the Moiré vectors (black arrows). The large diffuse feature in the lower-left quadrant is due to secondary electron emission (Ref. 38).

sample was moved, spots in the LEED pattern were observed to rotate relative to one another (see movie in supplementary material),[30] thus indicating that the hybrid films have regions of varying twist angle.

Figure 2(a) shows a representative LEED pattern of hybrid bilayer on H-terminated SiC with a twist angle of ~43°. In Fig. 2(b), this same pattern is shown along with the corresponding lattice vectors for both the over- and underlayer and a schematic representation of the way in which the angles are deduced. The strong hexagonal 1 × 1 diffraction spots marked by the blue circles in Fig. 2(b) originate from the graphene overlayer, whereas the weaker 1 × 1 spots labeled by the red circles are from the underlayer.[31] The distances between the specular beam and the 1 × 1 spots with blue and red circles are the same to within the experimental uncertainty. The overlayer versus underlayer assignment is verified by the observation that the underlayer pattern (red circles) does not change as the sample is translated under the electron beam. This static response is characteristic of the underlayer since the epitaxial graphene is monolithic and maintains a constant crystallographic arrangement relative to the SiC substrate.[21] In contrast, the overlayer (CVD graphene) does not maintain a constant arrangement relative to the copper, and thus its diffraction pattern (blue circles) rotates as the sample is examined in different locations.

Figure 2(c) shows a LEED pattern from the hybrid bilayer on C-layer-terminated graphene with a twist angle of 39.5°. The additional features surrounding the specular beam are due to the $6\sqrt{3} \times 6\sqrt{3}$ cos 30° LEED spots from the C-layer (marked by the red broken circles in Fig. 2(d)). This $6\sqrt{3} \times 6\sqrt{3}$ cos 30° LEED pattern gives further substantiation for the assignment of over- and underlayers. For example, in Fig. 2(c), the $6\sqrt{3} \times 6\sqrt{3}$ cos 30° C-layer spots and the weaker 1 × 1 graphene spots are shifted by 30°. This shift is characteristic of the rotation between the C-layer and monolayer of epitaxial graphene, thereby confirming the weaker 1 × 1 graphene spots as the epitaxial underlayer for all samples.[32] As a result, the twist angle can be defined as an angular shift between strong and weak 1 × 1 graphene spots. Finally, to show the range of angles observed in our analysis, Fig. 2(e) displays another example of a hybrid bilayer on H-terminated SiC with, in this case, a much smaller twist angle of ~2.5°.

The diffraction patterns in Fig. 2 include additional spots denoted by black circles that are not assigned to either graphene lattices or the C-layer. We conclude that these additional spots originate from Moiré structures most often observed in twisted graphene films using scanning tunneling microscopy.[10,33] Moiré structures evolve due to interference between the overlayer and underlayer and can be explained by a combination of the reciprocal lattice vectors of the two graphene lattices as follows.

In Fig. 2(b), we define the underlayer graphene as a reference having reciprocal lattice vectors G_K and $G_{K'}$ (red arrows). Similarly, the rotated overlayer is described using reciprocal lattice vectors $G_{K\vartheta}$ and $G_{K'\vartheta}$ (blue arrows). Using these four vectors, one can construct the Moiré structure from their differences as is shown schematically in Fig. 2(b) using $\Delta G_{K1} = G_{K\vartheta} - G_K$ and $\Delta G_{K2} = G_{K'\vartheta} - G_K$ and equivalently $\Delta G_{K1'}$ and $\Delta G_{K2'}$. Linear combinations of these difference (Moiré) vectors, ΔG_{K1} and $\Delta G_{K1'}$, can be used to specify the additional diffraction spots outlined by the larger hexagon, whereas those of ΔG_{K2} and $\Delta G_{K2'}$ describe the spots of the smaller hexagon. It is clear that when the twist angle is small, the Moiré spots move close to the specular beam as shown in Fig. 2(e). Combinations of these four Moiré vectors, meanwhile, allow for the designation of additional observed features. As such, all diffraction spots can be specified as originating from the underlayer and overlayer of graphene, the C-layer, the Moiré structure, and their combinations. In total, we therefore conclude that the hybrid bilayers made via transfer process are composed of series of TBG with varying stacking misorientations.

Finally, it is of note that the LEEM-IV trace and the sharp LEED patterns observed from the TBG films made via transfer are notably different from those of graphene layers transferred onto silicon wafers covered with silicon oxide.[34] We suggest that the atomically flat morphology of the epitaxial graphene underlayer is essential for obtaining an intimate contact between the two graphene sheets and is the source of this discrepancy. This is analogous to the significantly higher mobility[35] and flat morphology[36,37] of graphene on hexagonal boron-nitride as compared to silicon oxide.

To assess the extent over which a given twist angle persists, the domain structure of the hybrid bilayer films was studied using dark-field imaging from LEEM. Dark-field LEEM imaging uses the nonspecular electron reflection to image the surface and is thus able to identify the area associated with a particular diffraction spot. By translating the sample beneath the beam and employing this method, the domain size of the TBG was found to be on the order of a few tens of

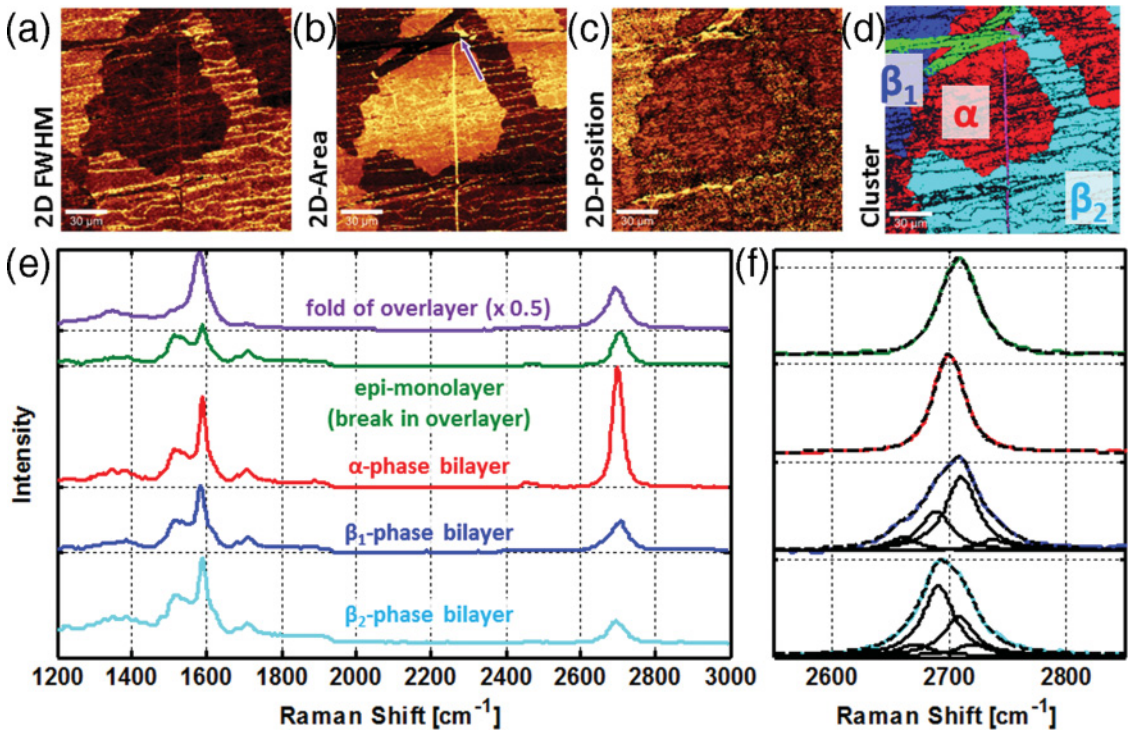

FIG. 3. (Color online) Micro-Raman spectroscopy of a hybrid bilayer graphene film on C-layer-terminated SiC. (a) False-color image of 2D-band FWHM map. Color scale; bright: 28 cm^{-1}, dark: 95 cm^{-1}. Scan size is 120 × 120 μm^2. (b) False-color map of 2D-band area under the curve. The purple arrow highlights the purple cluster shown in (d). (c) False-color map of 2D-band position. Color scale; bright: 2715 cm^{-1}, dark: 2690 cm^{-1}. (d) Image of clusters categorized by the different spectral features of the 2D-band (see text). (e) Representative Raman spectra of each cluster shown in (d). The Raman intensity is normalized to the SiC feature at ∼1700 cm^{-1}, except for the top spectrum (shown in purple), which is reduced by factor of two after the normalization. (f) 2D-band spectra of four prominent clusters with corresponding fits using Lorentzian functions (black lines). Labels and color of the spectra in (e) and (f) correspond to each cluster in (d).

microns, a size consistent with the grains of the original CVD overlayer and with that measured by Raman spectroscopy (see following). Therefore, domain size in the hybrid bilayer is determined by the characteristics of the CVD overlayer.

Further investigation into the domain size and the impact of the stacking sequence in TBG was conducted using confocal micro-Raman spectroscopy via the utilization of an excitation wavelength of 532 nm and a 100 × /0.9 numerical aperture (NA) objective.[39] We note that the locations investigated using Raman spectroscopy are not the same as those investigated using LEED/LEEM, but they are instead located nearby on the same sample(s). The hybrid bilayer films exhibit the characteristic Raman responses of both the G- (∼1590 cm^{-1}) and 2D (G')-bands (∼2700 cm^{-1}) of graphene along with features from the underlying SiC substrate. The D-band (∼1350 cm^{-1}) response characteristic of disruptions in the periodicity of the lattice, however, is marginal across the film, indicating that the transfer process has not appreciably damaged either the over- or underlayer.

Figure 3(a) to 3(c) shows Raman images derived from the full width at half maximum (FWHM), the area under the curve, and the position of the 2D-band (∼2700 cm^{-1}) for a hybrid bilayer film on C-layer-terminated SiC. The overall morphology resembles the LEEM image shown in Fig. 1(a) characterized by a train of micron-wide terraces separated by bunched steps of the SiC substrate where trilayer graphene is concentrated.

In addition to identifying those regions of trilayer graphene (bright stripes in Fig. 3(a)), the spectral images also allow for the specification of different regions within the bilayer portions of the film. The 2D-FWHM image in Fig. 3(a), for example, exhibits two regions having either a wide (bright) or narrow (dim) response. To further discriminate, the same bilayer regions shown in Fig. 3(a) are then divided into two additional regions through the analysis of the 2D-band area [Fig. 3(b)], where "stripes" of the material having either a noticeably large (bright, see purple arrow in Fig. 3(b)) or small (dim, green regions of Fig. 3(d)) 2D-band response are observed. Finally, the areas having a wide FWHM response (bright regions in Fig. 3(a)) are observed to have markedly different 2D-band positions in Fig. 3(c), thereby allowing for further demarcation.

In total, the categorization deduced from Fig. 3(a) to 3(c) allows for the specification of six different clusters, each having a distinct spectral response [Fig. 3(e)], which are spatially distributed as shown in Fig. 3(d). The narrow black cluster of Fig. 3(d) that persists across the entirety of the surface corresponds to trilayer graphene or thicker. As the focus of this work is on bilayer graphene, the black cluster is not discussed in further detail. From a geometrical argument, the narrow purple cluster (extending from the top to the bottom in the center of Fig. 3(d)) can be identified as a fold of the overlayer graphene since it continues even across the bunched steps originating from the SiC substrate. Its spectrum, shown

in Fig. 3(e), includes rather intense G-bands compared to the features of the SiC substrate, further corroborating this assignment. The green cluster, meanwhile, has a spectrum very similar to that of an epitaxial monolayer graphene on C-layer-terminated SiC. Specifically, it exhibits a 2D line-shape fit by a single Lorentzian function with a position in line with the epitaxial graphene we examined previously.[40] Additionally, the G-band has a lower intensity relative to the other clusters. We therefore presume that the green cluster is a break in the overlayer, exposing epitaxial monolayer to the surface. We note that the geometry of the green cluster also resembles that of typical breaks in the overlayers observed with LEEM (not shown).

We now focus on the three clusters covering the majority of the surface denoted as α, β_1, and β_2. By comparing their shapes and sizes to the domains of different stacking sequences observed via dark-field LEEM imaging, we deduce that each of these three clusters is bilayer graphene with differing twist angles, a fact that is supported by the distinctively different 2D-band line shapes of the three clusters. These line shapes originate from the double-resonance Raman process and provide direct insight into the electronic dispersion.[41] In the double-resonance process, excited electrons (holes) are scattered between inequivalent corners of the Brillouin zone (i.e., K & K') by phonons. The participating phonons have a wave vector that is determined based upon the distance in momentum space of the excited electron (holes) from the K-point of the Brillouin zone. This distance is a function of the electronic dispersion and the energy of the laser inducing the electronic transition. Therefore, changes in the electronic dispersion near the K-point, such as what occurs with variations in stacking sequence, should manifest themselves through changes in the 2D-band response.

The 2D line shapes of the α, β_1, and β_2 clusters are shown in Fig. 3(f) along with that of epitaxial monolayer on SiC. The most distinct line shape is that of the α-phase, which can be fit well to a single Lorentzian function (34 cm^{-1}, shown as a red line in Fig. 3(f)). This FWHM is narrower than that of the epitaxial monolayer graphene on C-layer-terminated SiC (37 cm^{-1}, shown as a green line in Fig. 3(f)). Similar narrowing of the 2D-FWHM in TBG has been reported previously when the folds of the exfoliated graphene have been examined.[20,42] In this case, the sharp Lorentzian feature was attributed to the similarity of the TBG's electronic dispersion to that of monolayer graphene. We therefore conclude that the α-phase exhibits a monolayer-like electronic dispersion of TBG with a particular, unspecified, twist angle. Finally, it is worth mentioning that a recent study of TBG realized from the exfoliation of multilayer graphene grown on SiC $(000\bar{1})$ indicated that the peak position and FWHM of the monolayer-like 2D-band could vary across the film.[43] We have not observed such drastic variations of the spectra as reported, but we do not exclude the possibility that a similar variation could be found in our hybrid TBG samples.

Unlike the 2D-bands of the α-cluster and monolayer graphene, the β_1 and β_2 clusters are qualitatively different, requiring four Lorentzian functions of equal width to describe their line shape [Fig. 3(f)]. This distinct response is similar to that of Bernal-stacked bilayers in which the π-state splits into two separate bands. Depending on the twist angle of TBG, the π-state is also expected to split in a manner qualitatively similar to that of Bernal bilayers.[6,41] The most notable difference between 2D-bands of β_1 and β_2 clusters is the separation between the four Lorentzian functions and thus the overall peak widths. The four peaks of the β_1 cluster are located at 2661, 2689, 2711, and 2739 cm^{-1}, with each peak having a common width of 33 cm^{-1}. On the other hand, the 2D-band of the β_2 cluster can be fit to peaks at 2670, 2691, 2709, and 2723 cm^{-1}, with a common width of 32 cm^{-1}. The separations among the 2D-band peaks for the β_1 cluster (28, 22, and 28 cm^{-1}) are notably larger than those of the β_2 cluster (21, 18, and 14 cm^{-1}), suggesting a larger splitting of π-states in momentum. In comparison, the reported separations of the 2D-band for exfoliated Bernal bilayer graphene using 532 nm excitation are 31, 18, and 16 cm^{-1}.[44]

The 2D line shapes of the β_1 and β_2 clusters are different than previous Raman measurements of TBG, where only a single Lorentzian response like that of the α phase has been reported.[13,19] With the appreciable difference in the 2D-band line shapes, we argue that the Raman response of the β_1 and β_2 clusters suggests notable interlayer splitting of the π-states, where at least one of these clusters has a stacking sequence different from that of Bernal stacking. It is, however, impossible to unequivocally substantiate this claim without knowing actual twist angles (a fact not obtainable using Raman alone) or the detailed electronic dispersions of the analyzed regions. At a minimum, however, the gross difference between the 2D line shapes of the α and β regions indicates that the electronic dispersion is modified by the twist angles due to the alteration in interlayer interactions that arise with misorientation.

Finally, we believe that the changes in the 2D line shapes arise from the twist angle and not from strain effects that may result from the growth or transfer processes. For each of the differing clusters, we observe that both the G- and 2D-bands have similar positions at $\sim$1590 and $\sim$2700 cm^{-1}, respectively. The similar peak positions among TBG domains suggest a nearly equivalent strain state across the entirety of the film. Additionally, the Raman response of graphene does not show any sign of splitting as would occur if the over- and underlayers were decoupled. This provides further support that the transferred overlayer is tightly bound to the underlayer in the hybrid bilayer films, similar to what is observed in bulk graphite.

IV. SUMMARY

By transferring CVD monolayer graphene onto epitaxially synthesized graphene on SiC, hybrid films of twisted bilayer graphene have been realized with several regions of differing in-plane misorientation. Employing a combination of low-energy electron microscopy (LEEM) and low-energy electron diffraction (LEED) along with Raman spectroscopy, we show that the hybrid bilayer films have intimate interlayer interaction, resulting in both long-range atomic ordering and variations in the electronic dispersion arising from the various twist angles. These films, therefore, offer a unique platform to study the effect of stacking misorientation on the electronic properties of bilayer graphene, while also suggesting the possibility of transfer processes as a means to

achieve graphene multilayers with the unique two-dimensional electronic properties of monolayer graphene.

ACKNOWLEDGMENTS

The work at Sandia National Laboratories was supported by Laboratory Directed Research and Development and by the US Department of Energy (DOE) Office of Basic Energy Sciences, Division of Materials Science and Engineering. A portion of this work was performed at CINT, a US DOE Office of Basic Energy Sciences user facility. Sandia National Laboratories is a multiprogram laboratory managed and operated by Sandia Corporation, a wholly owned subsidiary of Lockheed Martin Corporation, for the US Department of Energy's National Nuclear Security Administration under contract DE-AC04-94AL85000. We are grateful to Guild Copeland and Anthony McDonald for sample preparation and characterization. The work at Naval Research Laboratory was funded by the Office of Naval Research. We are also grateful to Glen G. Jurnigan and coworkers at NRL for sharing their manuscript prior to publication.[45]

*tohta@sandia.gov

[1] Y.-M. Lin, C. Dimitrakopoulos, K. A. Jenkins, D. B. Farmer, H.-Y. Chiu, A. Grill, and P. Avouris, Science **327**, 662 (2010).
[2] F. Xia, T. Mueller, R. Golizadeh-Mojarad, M. Freitag, Y.-m. Lin, J. Tsang, V. Perebeinos, and P. Avouris, Nano Lett. **9**, 1039 (2009).
[3] F. Xia, T. Mueller, Y. Lin, A. Valdes-Garcia, and P. Avouris, Nature Nanotech. **4**, 839, (2009).
[4] G. g. F. Schneider, S. W. Kowalczyk, V. E. Calado, G. g. Pandraud, H. W. Zandbergen, L. M. K. Vandersypen, and C. Dekker, Nano Lett. **10**, 3163 (2010).
[5] E. McCann and V. I. Fal'ko, Phys. Rev. Lett. **96**, 086805 (2006).
[6] E. J. Mele, Phys. Rev. B **81**, 161405 (2010).
[7] J. M. B. Lopes dos Santos, N. M. R. Peres, and A. H. Castro Neto, Phys. Rev. Lett. **99**, 256802 (2007).
[8] R. Bistritzer and A. H. MacDonald, Phys. Rev. B **81**, 245412 (2010).
[9] R. Bistritzer and A. H. MacDonald, Proc. Natl. Acad. Sci. **108**, 12233 (2011).
[10] J. Hass, F. Varchon, J. E. Millán-Otoya, M. Sprinkle, N. Sharma, W. A. de Heer, C. Berger, P. N. First, L. Magaud, and E. H. Conrad, Phys. Rev. Lett. **100**, 125504 (2008).
[11] S. Shallcross, S. Sharma, E. Kandelaki, and O. A. Pankratov, Phys. Rev. B **81**, 056803 (2010).
[12] Y. Wang, Z. Ni, L. Liu, Y. Liu, C. Cong, T. Yu, X. Wang, D. Shen, and Z. Shen, ACS Nano **4**, 4074 (2010).
[13] G. Trambly de Laissardière, D. Mayou, and L. Magaud, Nano Lett. **10**, 804 (2010).
[14] S. Shallcross, S. Sharma, and O. A. Pankratov, Phys. Rev. Lett. **101**, 56803 (2008).
[15] E. Mele, J. Phys. D: Appl. Phys., e-print arXiv:1109.2008 (to be published).
[16] E. J. Mele, Phys. Rev. B **84**, 235439 (2011).
[17] C. Berger, Z. Song, X. Li, X. Wu, N. Brown, C. Naud, D. Mayou, T. Li, J. Hass, and A. N. Marchenkov, Science **312**, 1191 (2006).
[18] C. Faugeras, A. Nerriere, M. Potemski, A. Mahmood, E. Dujardin, C. Berger, and W. de Heer, Appl. Phys. Lett. **92**, 011914 (2008).
[19] Z. Ni, Y. Wang, T. Yu, Y. You, and Z. Shen, Phys. Rev. B **77**, 235403 (2008).
[20] P. Poncharal, A. Ayari, T. Michel, and J. L. Sauvajol, Phys. Rev. B **78**, 113407 (2008).
[21] K. V. Emtsev, A. Bostwick, K. Horn, J. Jobst, G. L. Kellogg, L. Ley, J. L. McChesney, T. Ohta, S. A. Reshanov, and J. Röhrl, Nat. Mater. **8**, 203 (2009).
[22] C. Virojanadara, M. Syväjarvi, R. Yakimova, L. I. Johansson, A. A. Zakharov, and T. Balasubramanian, Phys. Rev. B **78**, 245403 (2008).
[23] C. Riedl, C. Coletti, T. Iwasaki, A. A. Zakharov, and U. Starke, Phys. Rev. Lett. **103**, 246804 (2009).
[24] T. Ohta, N. C. Bartelt, S. Nie, K. Thürmer, and G. L. Kellogg, Phys. Rev. B **81**, 121411 (2010).
[25] K. Lee, S. Kim, M. S. Points, T. E. Beechem, T. Ohta, and E. Tutuc, Nano Lett. **11**, 3624 (2011).
[26] X. Li, C. W. Magnuson, A. Venugopal, R. M. Tromp, J. B. Hannon, E. M. Vogel, L. Colombo, and R. S. Ruoff, J. Am. Chem. Soc. **133**, 2816 (2011).
[27] LEEM-III, Elmitec Elektronenmikroskopie GmbH.
[28] T. Ohta, F. El Gabaly, A. Bostwick, J. L. McChesney, K. V. Emtsev, A. K. Schmid, T. Seyller, K. Horn, and E. Rotenberg, New J. Phys. **10**, 023034 (2008).
[29] H. Hibino, H. Kageshima, F. Maeda, M. Nagase, Y. Kobayashi, and H. Yamaguchi, Phys. Rev. B **77**, 075413 (2008).
[30] See Supplemental Material at http://link.aps.org/supplemental/10.1103/PhysRevB.85.075415 for a movie showing the LEED patterns of the overlayer and underlayer rotating with respect to one another as the sample is moved beneath the electron beam.
[31] S. Nie, A. L. Walter, N. C. Bartelt, E. Starodub, A. Bostwick, E. Rotenberg, and K. F. McCarty, ACS Nano **5**, 2298 (2011).
[32] K. V. Emtsev, F. Speck, T. Seyller, L. Ley, and J. D. Riley, Phys. Rev. B **77**, 155303 (2008).
[33] J. Hicks, M. Sprinkle, K. Shepperd, F. Wang, A. Tejeda, A. Taleb-Ibrahimi, F. Bertran, P. Le Fèvre, W. A. de Heer, C. Berger, and E. H. Conrad, Phys. Rev. B **83**, 205403 (2011).
[34] K. R. Knox, S. Wang, A. Morgante, D. Cvetko, A. Locatelli, T. O. Mentes, M. A. Niño, P. Kim, and R. M. Osgood Jr., Phys. Rev. B **78**, 201408 (2008).
[35] C. R. Dean, A. F. Young, I. Meric, C. Lee, L. Wang, S. Sorgenfrei, K. Watanabe, T. Taniguchi, P. Kim, K. L. Shepard, and J. Hone, Nat. Nano **5**, 722 (2010).
[36] W. Gannett, W. Regan, K. Watanabe, T. Taniguchi, M. Crommie, and A. Zettl, Appl. Phys. Lett. **98**, 242105 (2011).
[37] J. Xue, J. Sanchez-Yamagishi, D. Bulmash, P. Jacquod, A. Deshpande, K. Watanabe, T. Taniguchi, P. Jarillo-Herrero, and B. J. LeRoy, Nat. Mater. **10**, 282 (2011).
[38] H. Hibino, H. Kageshima, F. Z. Guo, F. Maeda, M. Kotsugi, and Y. Watanabe, Appl. Surf. Sci. **254**, 7596 (2008).
[39] Alpha300 RAS microscope, WITec GmbH.
[40] D. A. Schmidt, T. Ohta, and T. E. Beechem, Phys. Rev. B **84**, 235422 (2011).

[41] A. C. Ferrari, J. C. Meyer, V. Scardaci, C. Casiraghi, M. Lazzeri, F. Mauri, S. Piscanec, D. Jiang, K. S. Novoselov, S. Roth, and A. K. Geim, Phys. Rev. Lett. **97**, 187401 (2006).

[42] Z. Ni, L. Liu, Y. Wang, Z. Zheng, L.-J. Li, T. Yu, and Z. Shen, Phys. Rev. B **80**, 125404 (2009).

[43] D. S. Lee, C. Riedl, T. Beringer, A. H. Castro Neto, K. von Klitzing, U. Starke, and J. H. Smet, Phys. Rev. Lett. **107**, 216602 (2011).

[44] L. Malard, M. Pimenta, G. Dresselhaus, and M. Dresselhaus, Phys. Rep. **473**, 51 (2009).

[45] G. G. Jernigan, T. J. Anderson, J. T. Robinson, J. D. Caldwell, J. C. Culbertson, M. G. Ancona, V. D. Wheeler, L. O. Nyakiti, R. Myers-Ward, A. L. Davidson, A. L. Friedman, P. M. Campbell, and D. K. Gaskill, "Bilayer graphene by bonding CVD graphene to epitaxial graphene" (accepted for publication, 2012).